VER
Vascular & Endovascular Review

Formulation and Evaluation of a Bioinspired Nanogel Containing Silver Nanoparticles Synthesized Using Bacillus licheniformis

Ms. Jayshri T. Swami[1], Dr. Nagoba Shivappa[1]*

[1]Research Scholar, Centre for Research in Pharmaceutical Sciences (CRPS), Channabasweshwar Pharmacy College (Degree), Latur, 413512, Maharashtra, India
swamijayashri520@gmail.com, https://orcid.org/0000-0002-1777-5940
[1]*Professor, Centre for Research in Pharmaceutical Sciences (CRPS), Channabasweshwar Pharmacy College (Degree), Latur, 413512, Maharashtra, India
Email Id: nagobashivraj@gmail.com, https://orcid.org/0000-0000-0001-7895-3088

***Corresponding Author:**
Dr. Nagoba Shivappa N.
Centre for Research in Pharmaceutical Sciences (CRPS),
Channabasweshwar Pharmacy College (Degree), Latur, 413512, Maharashtra, India
Email: nagobashivraj@gmail.com

ABSTRACT

Nanotechnology-based drug delivery systems have emerged as promising strategies to address the limitations of conventional therapies, including poor solubility, rapid clearance, and nonspecific distribution. Bioinspired nanomedicine synthesized using microorganism's offers enhanced biocompatibility, safety, and environmental sustainability. In this study, Bacillus licheniformis, a non-pathogenic bacterium, was utilized for the extracellular synthesis of silver nanoparticles (AgNPs) exhibiting excellent antimicrobial activity and stability. These biosynthesized AgNPs were incorporated into a nanogel a three-dimensional hydrophilic polymeric network known for high drug-loading capacity, controlled release, and improved retention at the target site. The nanogel formulation was optimized to enhance therapeutic efficacy, tissue penetration, and wound-healing potential. Comprehensive evaluation, including physicochemical characterization, in-vitro analysis, and in-vivo wound-healing studies using excision and incision models in albino Wistar rats, revealed significant wound contraction, accelerated epithelialization, and increased tensile strength compared to control and standard treatments. Overall, the findings demonstrate that B. licheniformis-derived AgNP-loaded nanogels represent a promising, eco-friendly, and efficient platform for targeted drug delivery and advanced wound-healing applications.

KEYWORDS: Nanogel, Bacillus licheniformis, silver nanoparticles, bioinspired nanomedicine, wound healing.

How to Cite: Ms. Jayshri T. Swami, Dr. Nagoba Shivappa, (2025) Formulation and Evaluation of a Bioinspired Nanogel Containing Silver Nanoparticles Synthesized Using Bacillus licheniformis, Vascular and Endovascular Review, Vol.8, No.16s, 373-376.

INTRODUCTION

Nanotechnology has become a powerful tool in contemporary drug-delivery research, offering solutions to challenges such as poor solubility, rapid systemic clearance, and nonspecific distribution associated with conventional therapeutic formulations. Within this field, bioinspired nanomedicine nanomaterials synthesized using biological organisms or biomolecules has gained significant interest due to its inherent biocompatibility, safety, sustainability, and cost-effectiveness. Among various biological systems, **Bacillus licheniformis**, a non-pathogenic and widely studied bacterium, has shown strong potential for the extracellular synthesis of silver nanoparticles (AgNPs). These biologically produced AgNPs are typically stable, biocompatible, and possess notable antimicrobial properties, making them attractive candidates for therapeutic use. The green synthesis approach further enhances their value by offering a simple, scalable process that avoids hazardous chemicals [1, 2].

To enhance the therapeutic performance of silver nanoparticles, they can be incorporated into **nanogels** three-dimensional, hydrophilic polymer networks on the nanoscale capable of absorbing large quantities of water or biological fluids. Their soft, adaptable structure promotes better interaction with biological tissues, improving retention and bioavailability at the target site. Nanogels provide numerous advantages, including high drug-loading efficiency, controlled and sustained release, enhanced nanoparticle stability, and potential for targeted delivery. Their inherent biocompatibility and biodegradability help minimize systemic toxicity, while the inclusion of silver nanoparticles imparts added antimicrobial and wound-healing properties. These characteristics make nanogels particularly suited for topical and transdermal applications where deep tissue penetration and prolonged therapeutic action are desired [3,4].
The present study focuses on developing and evaluating a bioinspired nanogel formulation incorporating AgNPs synthesized using **Bacillus licheniformis**. The aim is to create a stable, biocompatible, and efficient nanogel capable of

controlled drug release, enhanced wound healing, and reduced toxicity. Formulation optimization, physicochemical characterization, and both in-vitro and in-vivo evaluation, along with stability studies, will be conducted. Ultimately, this work seeks to establish B. licheniformis-derived silver nanoparticle nanogels as a robust platform for advanced therapeutic applications and targeted drug-delivery strategies [5].

MATERIALS AND METHODS

2.1 Materials: Most of the chemical's chitosan, acetic acid, glycerol, sodium hydroxide were procured from **Cosmo Chem. Pvt. Ltd.** and Research **Lab Fine Chem Industries**. Silver nitrate and Methanol were obtained from **Research Lab Fine Chem Industries** and **Solanki Enterprises**, while Sabouraud Dextrose Agar procured from HiMedia exclusively.

2.2 Method for Preparation of bioinspired Nano gel [7-11]

a. The nanogel was formulated using a cold mechanical method with varying concentrations of chitosan.
b. The required amount of polymer was accurately weighed and gradually sprinkled onto aqueous over a period of approximately 2 hours.
c. Chitosan was dissolved in 1% aqueous acetic acid and allowed to swell completely.
d. After swelling, the chitosan dispersion was stirred on a magnetic stirrer. The specified quantity of nanoparticles was slowly incorporated into the mixture to promote gel formation. Propylene glycol and glycerin were then added, and the mixture was stirred at 500 rpm.
e. Stirring was continued until complete dispersion of chitosan was achieved, resulting in a uniform and homogeneous gel.
f. The final pH was adjusted to 6.1–6.8 using sodium hydroxide to ensure an aesthetically acceptable gel formulation.

2.3 Design of Experiment and Analysis By Quality By Design Approach

A Quality by Design (QbD) framework was employed to systematically optimize the Bioinspired Nano gel formulation variables using a Central Composite Design (CCD) within the Design-Expert® (Version 13, Stat-Ease Inc., USA) software. Two critical process parameters (CPPs) the concentration of Chitosan (%) and stirring speed (B, rpm) were selected based on prior screening and risk assessment (Ishikawa and FMEA analysis). The critical quality attributes (CQAs) defined were particle size (nm), zeta potential (mV), and entrapment efficiency (%). Each factor was studied at five levels ($-\alpha, -1, 0, +1, +\alpha$) with $\alpha = 1.414$. A total of 12 experimental runs (including center-point replications) were performed as per the CCD matrix to explore linear, interaction, and quadratic effects. The bioinspired nanogel formulated according to standardized protocol, and the resulting formulations were characterized for particle size and zeta potential using a dynamic light scattering (DLS) system (Malvern Zetasizer Nano ZS), while entrapment efficiency was quantified by UV–visible spectroscopy after ultracentrifugation. All experiments were conducted in triplicate, and results were expressed as mean ± SD.

Table 1. Formulation batches of Nanogel

Formulation Code	Nanoparticle (mg)	Concentration of Chitosan (mg)	Stirring speed (rpm)
L1	20	1.5	500
L2	20	1.75	750
L3	20	2	500
L4	20	1.39645*	750
L5	20	1.75	396.447*
L6	20	2.10355*	750
L7	20	1.75	1103.55*
L8	20	2	1000
L9	20	1.5	1000

2.4Characterization of Nanogel [12-15]

2.4.1 Physical Examination: The prepared nanogel formulations were visually inspected and found to be transparent, crystal clear, and smooth in appearance.

2.4.2 Viscosity Measurement: Viscosity was determined using a Brookfield Rheometer (CCT-14 spindle). The spindle was immersed in the gel sample, and viscosity was recorded.

2.4.3 Spreadability: The spreadability of nanogel was checked by Spreadability method. A weighed amount of gel sample (500 mg) was placed carefully at the Centre of the circle (1 cm in diameter) on pre marked glass plate over which the second glass plate was placed. The weight of 0.5 kg was applied over upper glass plate for 5 min and increase in diameter from the initial value of gel was noted.

2.4.4 Homogeneity: Formulations were checked visually to assess uniformity and absence of aggregates.

2.4.5 Extrudability: Extrudability was tested by filling formulations into collapsible tubes and determining the weight (g) required to extrude a 0.5 cm ribbon of gel within 10 seconds.

2.4.6 Drug Content: Nanoparticle-loaded nanogel was dissolved in ethanol, sonicated (15 min), filtered, and scanned at 440 nm using a UV–Visible spectrophotometer to determine drug content.

2.4.7 Particle Size and Zeta Potential: Nanogel concentrations were diluted with distilled water, and twelve measurements were taken to obtain average values, Dynamic light scattering (Zetasizer) was used to measure particle size, and zeta potential.

2.4.8 Encapsulation Efficiency (EE%):- The Entrapment efficiency of silver nanoparticle loaded nanogel was determined indirectly by centrifuging at 12,000 rpm for 10 min. The supernatant was mixed with ethanol and analyzed at 440 nm using UV–Visible spectrophotometry (Shimadazu-1800) to quantify the unentrapped drug.
EE% was calculated using the formula
EE (%) = (Total Drug−Free Drug) /Total Drug X 100

2.4.9 Transmission Electron Microscopy (TEM): Surface morphology of the optimized batch was established by using Transmission Electron Microscopy (TEM).

2.4.10. PXRD Study: Powder X-ray diffraction (PXRD) of the optimized gel batch was carried out using Cu Kα radiation (λ = 1.542 Å) at 30 kV and 30 mA, over a 2θ range of 2–60°.

2.4.11 Differential Scanning Calorimetry (DSC): Thermal analysis of the nanogel was performed on a METTLER TOLEDO DSC. Samples (5–10 mg) were sealed in aluminium pans and heated from 0–300 °C at 10 °C/min under nitrogen purge (50 ml/min through cell, 100 ml/min through cooling unit).

2.4.12 In-vitro Drug diffusion:
The cellophane membrane diffusion technique was used to study the invitro diffusion of drug from prepared nanogel formulations. The receptor medium used was freshly prepared phosphate buffer (P^H 7.4). The cellophane membrane, soaked overnight in the receptor medium, was placed in the Franz diffusion cell assembly. A 0.5 gm sample of formulation was added to the donor compartment and the assembly was maintained at 37 ± 2 °C with stirring at 100 rpm, for 2 h. Samples were withdrawn at predetermined intervals, replaced with fresh medium, filtered, and analyzed spectrophotometrically at 440 nm[16].

2.4.13 Stability Study: The accelerated stability study was conducted as per ICH guideline Q_1A (R_2). The optimized nanogel was stored at room temperature for 3 months. No significant changes were observed in physical appearance, viscosity, or drug release profile, confirming formulation stability [17].

2.4.15 In-Vivo Wound Healing Study [19-22]

Table No. 2 Experimental design (Grouping)

Group I (F1=CONTROL)	Rats were subjected to Excision Wound using biopsy punch and treated with F1 for 21 days.
Group II (F2 =standard)	Rats were subjected to Excision Wound and treated with F2 for 21 days.
Group III (F3 =optimized formulation(L8)	Rats were subjected to Excision Wound and treated with F3 for 21 days.

- **Experimental Conditions**

Albino Wistar rats (180–200 g, female) were used, housed in standard metabolic cages (6 per cage) with free access to food and water under controlled environmental conditions. All experimental protocols were reviewed and approved by the Institutional Animal Ethical Committee.

- **Excision Wound Model Procedure**

Rats were anesthetized using ketamine (100 mg/kg, i.p.) in combination with xylazine (10 mg/kg, i.p.). A circular region measuring approximately 500 mm² was delineated on the dorsal surface, and a full-thickness excision wound was created using a biopsy punch. The wound dimensions were recorded on day 0 and subsequently monitored using a digital caliper. Measurements were taken at 7-day intervals until day 14, followed by assessments on alternate days until complete wound closure (19,20].
Wound contraction was determined using the formula:

$$\text{Wound Contraction } (\%) = \left(\frac{\text{Healed Area}}{\text{Initial Wound Area}} \right) \times 100$$

where:
Healed Area=Initial Wound Area−Current Wound Area
The duration of epithelialization, noted as the day on which the scab or eschar detached without leaving a raw surface, was recorded along with the final scar area.

RESULT AND DISCUSSION

- **Optimization of Nanogel Using QbD Approach**

The 9 experimental runs generated particle sizes ranging from 127 nm to 274 nm, zeta potentials between –21.8 mV and –29.5 mV, viscosity ranging from 14,520 to 17,025 cP, entrapment efficiencies from 68.53% to 88.21%& drug content from 85.42% to 95.45%. This variability confirmed the influence of both Chitosan concentration and stirring speed on nanogel characteristics.

Table3. Experimental formulation batches of nanogel prepared usingCentral Composite Design (CCD)

Formulation Code	Nanoparticle (mg)	Chitosan Concentration (mg)	Stirring Speed (rpm)
L1	20	1.50	500
L2	20	1.75	750
L3	20	2.00	500
L4	20	1.39645*	750
L5	20	1.75	396.447*
L6	20	2.10355*	750
L7	20	1.75	1103.55*
L8	20	2.00	1000
L9	20	1.50	1000

3.1 Evaluation of Rheological and Mechanical Attributes

3.1.1 Viscosity: The viscosity values of the formulations ranged from 14,520 to 17,025 cP, reflecting a substantial influence of formulation composition (Table 4). ANOVA confirmed the significance of the linear model (p=0.0252). Both chitosan concentration (A, p=0.0282) and stirring speed (B, p = 0.0472) had significant positive effects on viscosity, indicating that increased polymer ratio and higher mixing shear contribute to greater structural integrity of the gel network.

3.1.2

Model fit statistics demonstrated acceptable predictability:

- **R^2 =0.71**
- AdjustedR^2 =0.61
- PredictedR^2=0.59
- **C.V.=12.21%**
- Adequate Precision=6.57

The coded and actual equations describing the model are:

Coded factors:

Viscosity=15796.00+515.73A+446.40B

Actual factors:

Viscosity=10846.67364+2062.93378(Chitosan)+1.78559(Stirring speed)

The response surface (Figures1-3)clearly showed that viscosity increased sharply with risingchitosanconcentration,whilestirringspeedcontributedmoderately,likelyduetoshear- induced polymer chain alignment and enhanced entanglement.

Table 4.Viscosity of nanogel formulations (mean± SD)

Formulation	Viscosity(cP)
L1	14520 ± 0.145
L2	15719 ± 0.341
L3	16200 ± 0.001
L4	15890 ± 0.056
L5	14980 ± 0.084
L6	16230 ± 0.0925
L7	16540 ± 0.614
L8	17025 ± 0.002
L9	15060 ± 0.091

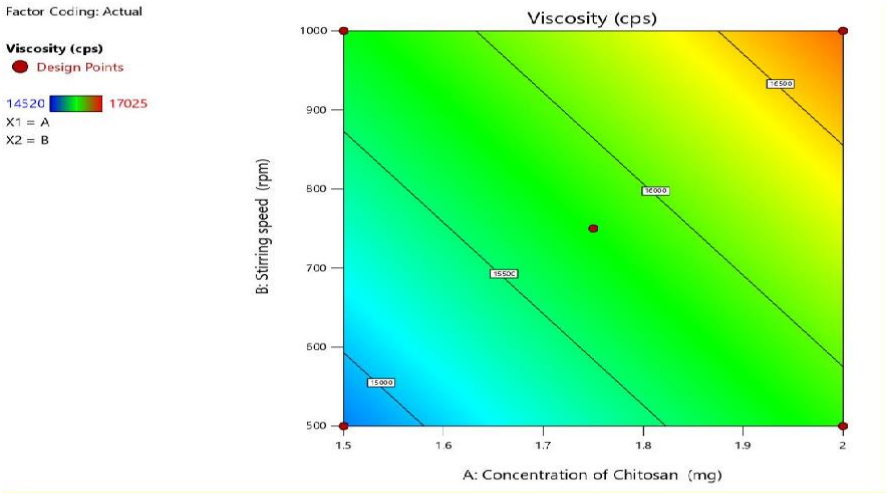

Figure1. Contour plot illustrating the interaction effect of Chitosan concentration (A) and Stirring speed (B) on the response variable of the nanogel formulation. The plot demonstrates the optimal region within the design space where the desired respo (appropriate viscosity) is achieved

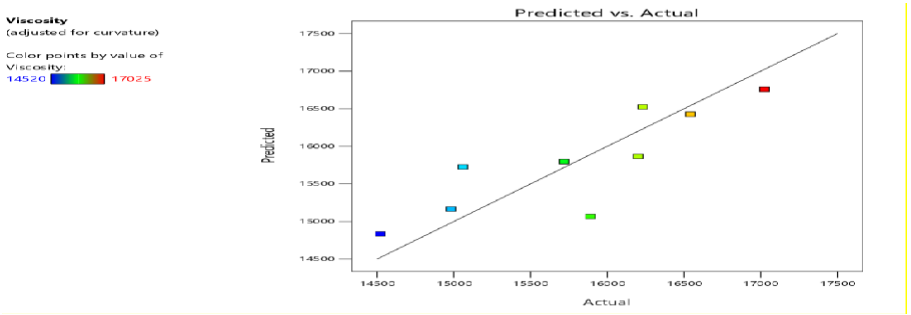

Figure2.Predicted versus actual plot showing the correlation between experimentally observed values and model-generated values for the nanogel response. The close clustering of data points along the diagonal line confirms the accuracy, reliability and goodness-of-fit of the developed statistical model

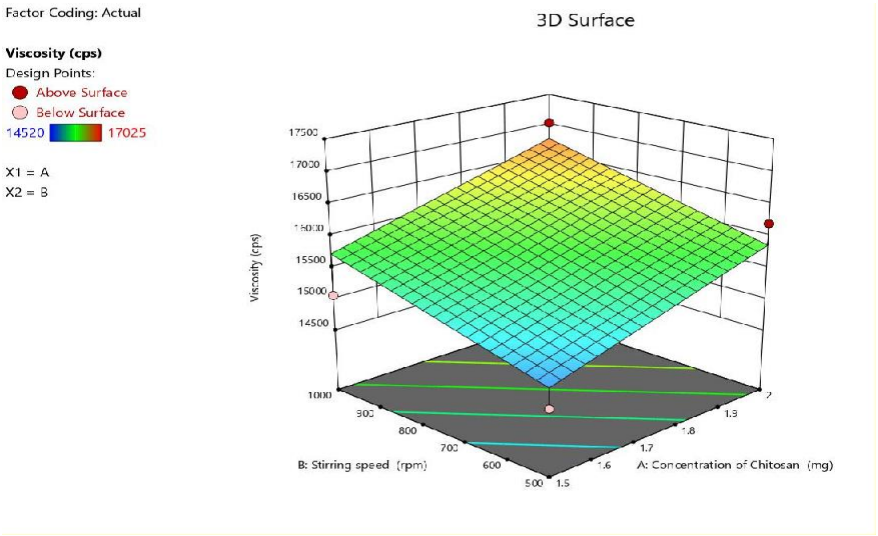

Figure3.Three-dimensional response surface plot depicting the combined influence of Chitosan concentration (A) and Stirring speed (B) on the nanogel response. The curvature of the surface illustrates how factor interactions affect the response and highlights the optimal operational region identified through QbD-based optimization

3.1.3 Spreadability, Homogeneity, and Extrudability: Spreadabilityvaluesrangedfrom5.8 to 8.4 g·cm/sec, with formulations L3 and L8 showing superior spreading behavior (Table 5). Higher spreadability corresponded inversely with viscosity, as expected for semi-solid systems. Homogeneity testing revealed that most formulations were uniform, with L3 and L8 rated as excellent, reflecting optimal polymer distribution (Table5). Extrudability testing demonstrated that L3 and L8 exhibited excellent extrusion properties, while L5 showed poor extrusion, correlating with its lower polymer content and weaker gel structure (Table 5).

Table5. Spreadability, homogeneity, and extrudability characteristics of the prepared nanogel formulations

Formulation	Spreadability (g·cm/sec) (mean±SD)	Homogeneity	Extrudability
L1	6.5 ± 0.2	Uniform	Moderate
L2	7.3 ± 0.2	Uniform	Good
L3	8.1 ± 0.3	Excellent	Excellent
L4	6.7 ± 0.2	Slightly non-uniform	Moderate
L5	5.8 ± 0.2	Moderate	Poor
L6	7.6 ± 0.2	Uniform	Good
L7	7.1 ± 0.3	Uniform	Good
L8	8.4 ± 0.2	Excellent	Excellent
L9	7.0 ± 0.2	Uniform	Good

3.1.4 Drug Content and Yield: Drug content ranged between 85.42% and 95.45%, with L8 demonstrating the highest encapsulation and yield (Table 6). Formulation yield varied from 79.9% to 92.1%, reflecting good reproducibility of the preparation process.

Table 6.Percentage yield and drug content of nanogels

Formulation	Yield (%)	Drug Content (%)
L1	81.2	88.56
L2	85.7	92.48
L3	92.1	93.24
L4	88.6	90.87
L5	79.9	91.56
L6	83.4	85.92
L7	82.7	89.63
L8	90.1	95.45
L9	87.3	85.42

3.2 Particle Size and Surface Charge Analysis

Table7. Particle size, PDI, and zeta potential of nanogel formulations

Formulation	Particle Size(nm)	PDI	Zeta Potential(mV)
L1	274.0	0.348	-22.5
L2	198.7	0.292	-27.4
L3	192.3	0.214	-23.6
L4	164.5	0.276	-28.2
L5	255.6	0.331	-21.8
L6	127.2	0.265	-30.1
L7	174.1	0.298	-25.9
L8	112.3	0.249	-29.5
L9	210.4	0.305	-26.3

3.2.1 Particle Size: The particle size ranged from 112.3to274nm, with formulation L8(112.3 nm) representing the optimized batch (Table 7, Fig. 4).The linear model for particle size was statistically significant ($p = 0.0374$), confirming the validity of the selected formulation parameters. ANOVA showed that:

- **Stirring speed (B)** significantly decreased particle size ($p = 0.0423$), attributed to increased shear leading to smaller nano droplets.
- **Chitosan concentration (A)** exhibited a mild, non-significant increasing effect ($p = 0.0603$), likely due to increased viscosity restricting efficient droplet breakup.

Model statistics indicated acceptable predictive power:

- **R^2 =0.6656**
- Adjusted R^2 =0.5541
- Predicted R^2=0.5448

- **C.V.=18.75%**
- Adequate Precision=5.977

Coded equation:

Particle size=189.90-29.07A-32.36B

Actual equation:

Particle size= 490.45516 -116.27595 (Chitosan)-0.129430 (Stirring speed)

Contour plots, predicted vs. actual graph, and 3D response surfaces (Figures 5-7) illustrate a distinct reduction in particle size with increasing stirring speed and moderate polymer concentration.

Figure 4.Particle size distribution of the optimized nanogel formulation (L8) measured by dynamic light scattering

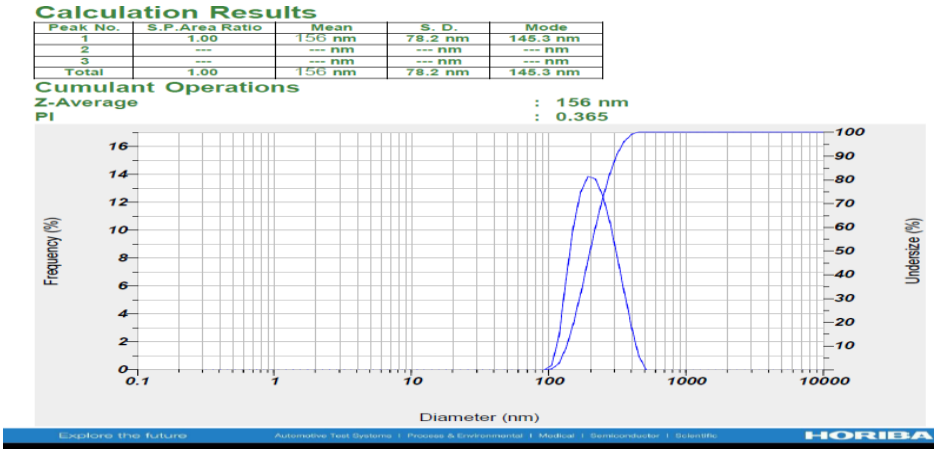

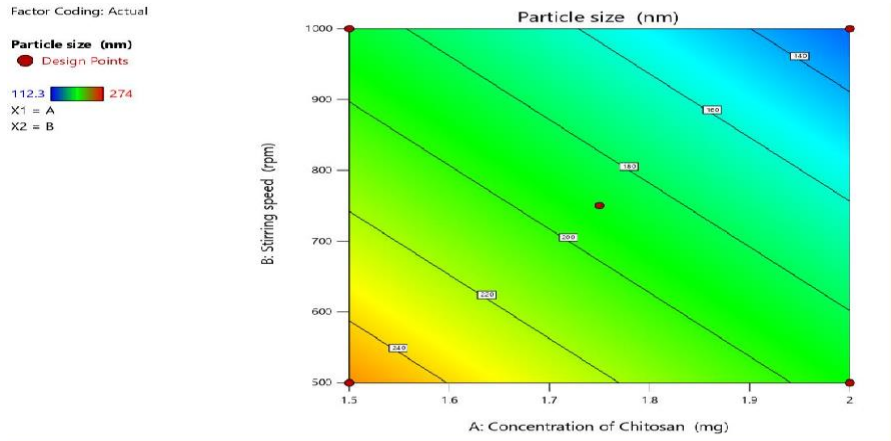

Figure 5. Contour plot illustrating the interaction effect of Chitosan concentration(A) and Stirring speed (B) on the response variable of the nanogel formulation. The plot demonstrates the optimal region within the design space where the desired response (minimum particle size) is achieved

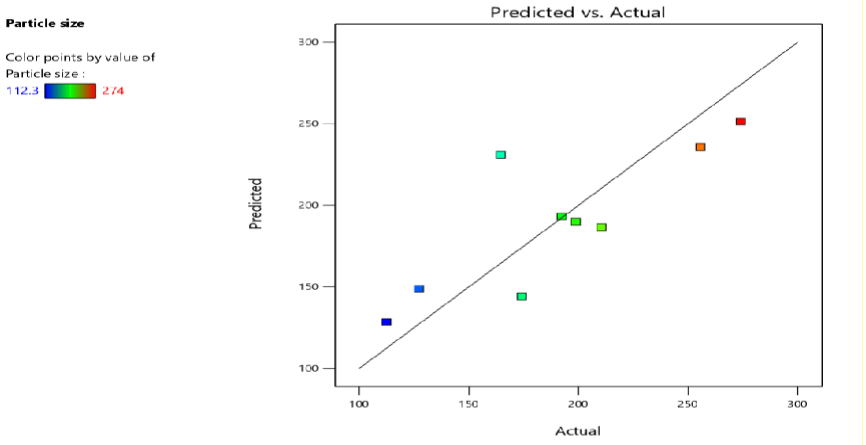

Figure6.Predicted versus actual plot showing the correlation between experimentally observed values and model-generated values for the nanogel response. The close clustering of data points along the diagonal line confirms the accuracy,reliability, and goodness-of-fit of the developed statistical model

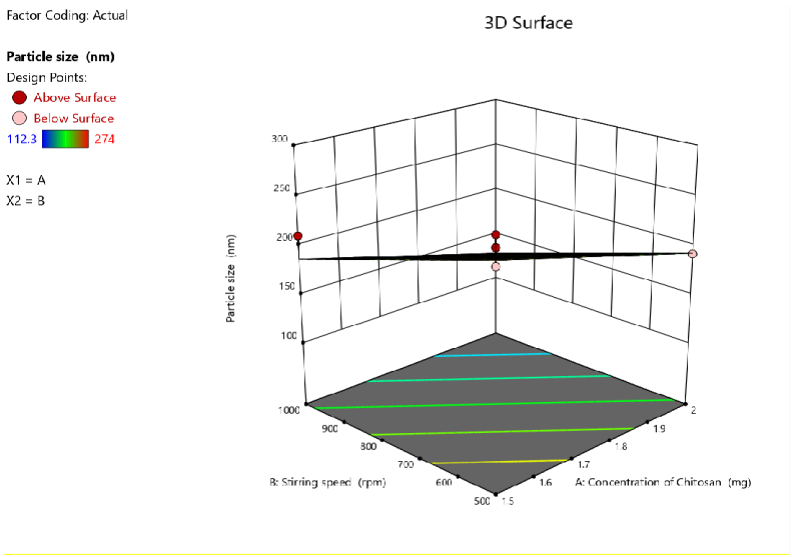

Figure7.Three-dimensional response surface plot depicting the combined influence of Chitosan concentration (A) and Stirring speed (B) on the nanogel response. The curvature of the surface illustrates how factor interactions affect the response and highlights the optimal operational region identified through QbD-based optimization

3.2.2 Zeta Potential: Zeta potential values ranged from -21.8 to -30.1 mV, confirming good electrostaticstabilityofthenanogel.TheoptimizedbatchL8exhibitedahighstabilityof-29.5 mV (Fig. 8). The quadratic model for zeta potential was significant (F = 9.30, p = 0.0479). Stirring speed(B)had the strongest effect on surface charge (p=0.0198), indicating that high shear enhances surface ionization and stabilizes the nanosystem.
Model statistics:

- **R^2 =0.9394**
- AdjustedR^2 =0.8384
- PredictedR^2=0.8215
- **C.V.=10.59%**
- Adequate Precision=9.4558

Codede quation:
Zeta Potential=-27.40–0.8734A-1.934B –0.5250AB-0.6187A^2+ 2.034B^2
Actual equation:

Zeta potential =- 38.53680+37.45646 (Chitosan)- 0.041800 (Stirring speed)
-0.008400(Chitosan×Stirring speed)-9.90000(Chitosan²)+0.000033 (Stirring speed²)

Response surface diagrams (Figures9-11)high light the non linear influence of chitosan and stirring speed on charge distribution.

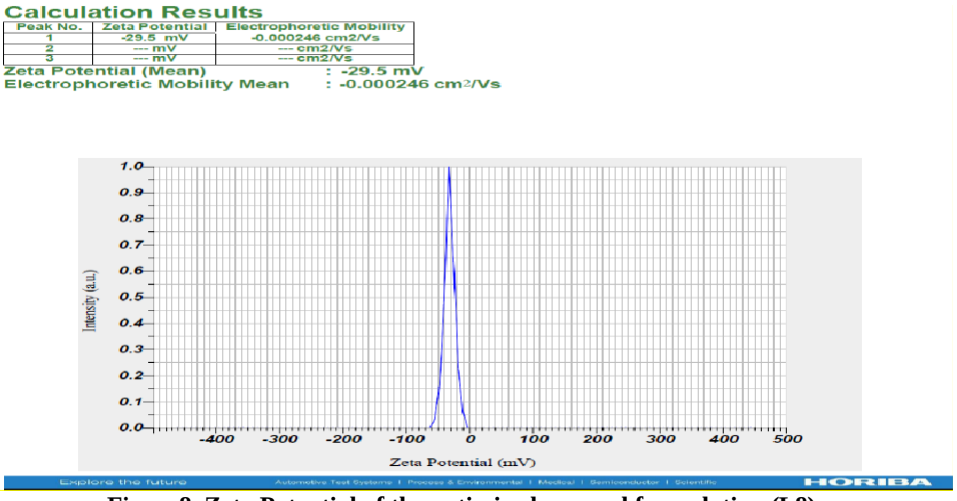

Figure8. Zeta Potential of the optimized nanogel formulation (L8)

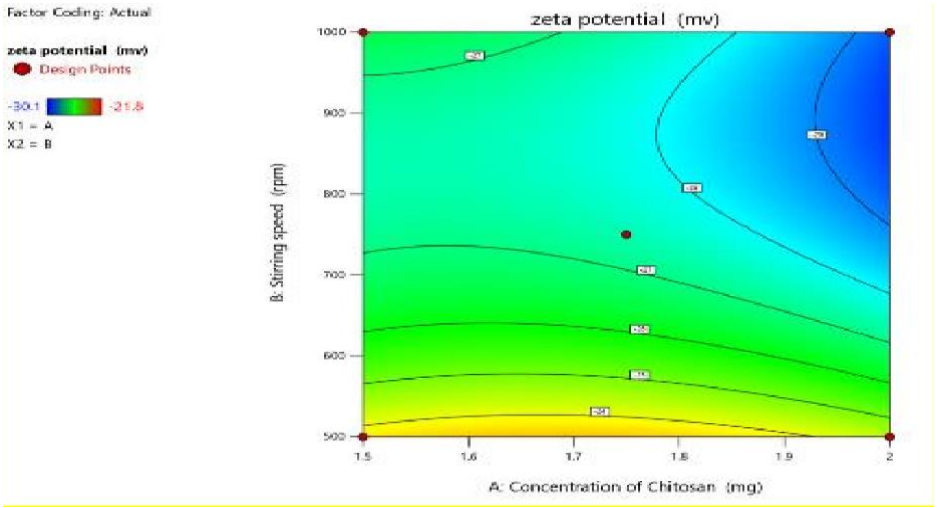

Figure9. Contour plot illustrating the interaction effect of Chitosan concentration (A) and Stirring speed (B) on the response variable of the nanogel formulation. The plot demonstrates the optimal region within the design space where the desired response (Zeta Potential) is achieved

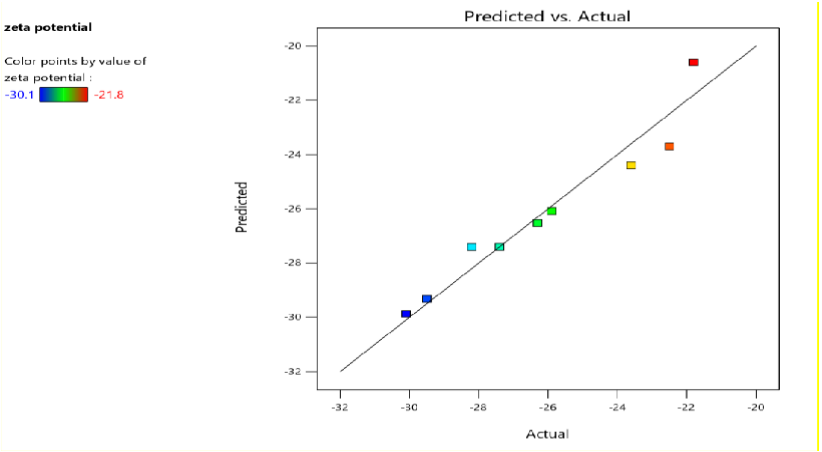

Figure10. Predicted versus actual plot showing the correlation between experimentally observed values and model-generated values for the nanogel response. The close clustering of data points along the diagonal line confirms the accuracy, reliability, and goodness-of-fit of the developed statistical model

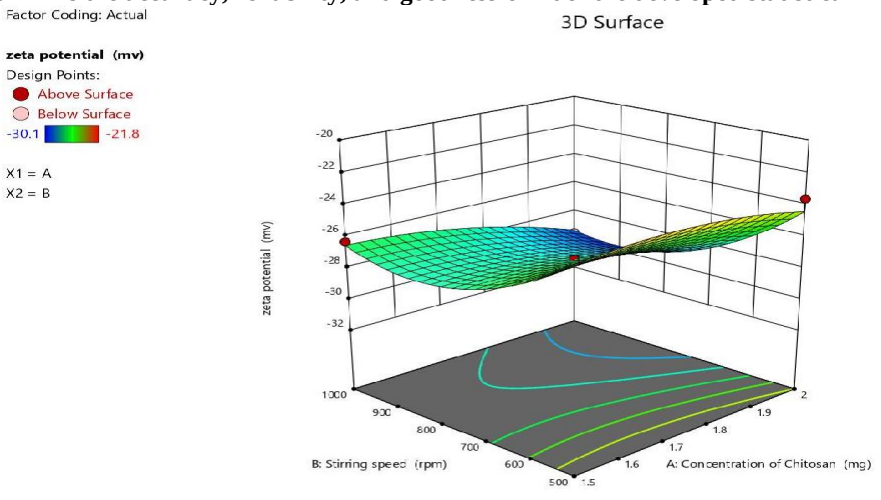

Figure11.Three-dimensional response surface plot depicting the combined influence of Chitosan concentration (A) and Stirring speed (B) on the nanogel response. The curvature of the surface illustrates how factor interactions affect the response and highlights the optimal operational region identified through QbD-based optimization.

3.3 Encapsulation Efficiency: Entrapment efficiency ranged between 68.53% and 91.45%, with the optimized formulation L8 showing the highest value (91.45%) (Table 8). ANOVA confirmed model significance (F = 6.94, p = 0.0275), with:

- **Chitosan concentration (A)** significantly increasing entrapment (p=0.0220)
- **Stirring speed (B)** negatively but non-significantly contributing (p=0.0788) Model fit parameters:
- **R^2 = 0.6982**
- Adjusted R^2 = 0.5976
- Predicted R^2 = 0.5812
- C.V.=10.57%

Coded equation:

Encapsulation Efficiency =80.05+5.70A-3.93B

Actual equation:

Encapsulation Efficiency =51.93754+22.79947(Chitosan)-0.015720(Stirring speed)

The contour, 3D surface, and predicted vs. actual plots (Figures 12-14) revealed that moderate chitosan concentrations improved encapsulation by forming denser polymeric networks around nanoparticles.

Table 8.Entrapment efficiency of nanogel formulations (mean±SD)

Formulation	Entrapment Efficiency (%)
L1	80.63 ± 0.02
L2	79.52 ± 0.256
L3	88.12 ± 0.478
L4	70.52 ± 0.198
L5	88.21 ± 0.0005
L6	81.26 ± 0.211
L7	72.18 ± 0.009
L8	91.45 ± 0.078
L9	68.53 ± 0.014

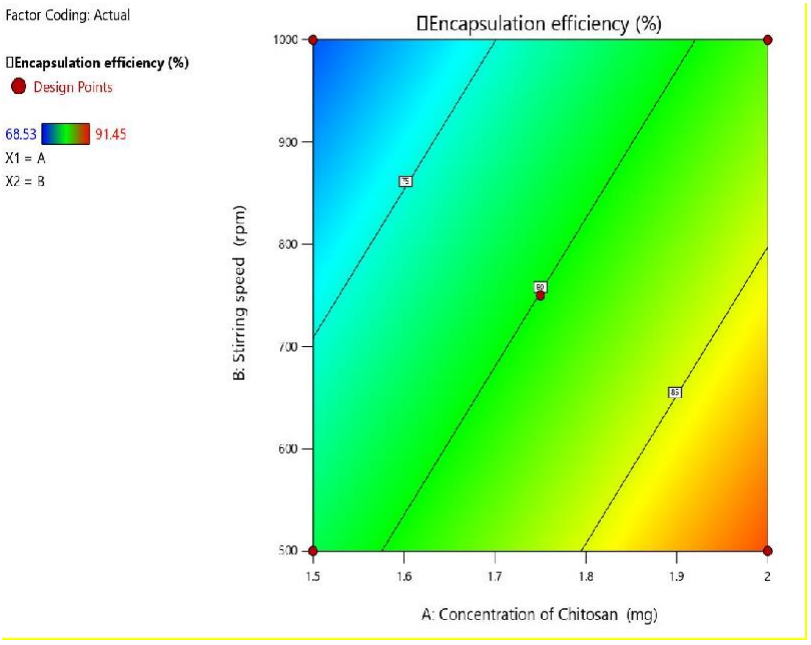

Figure12.Contour plot illustrating the interaction effect of Chitosan concentration (A) and Stirring speed (B) on the response variable of the nanogel formulation. The plot demonstrates the optimal region within the design space where the desired response (Entrapment Efficiency) is achieved

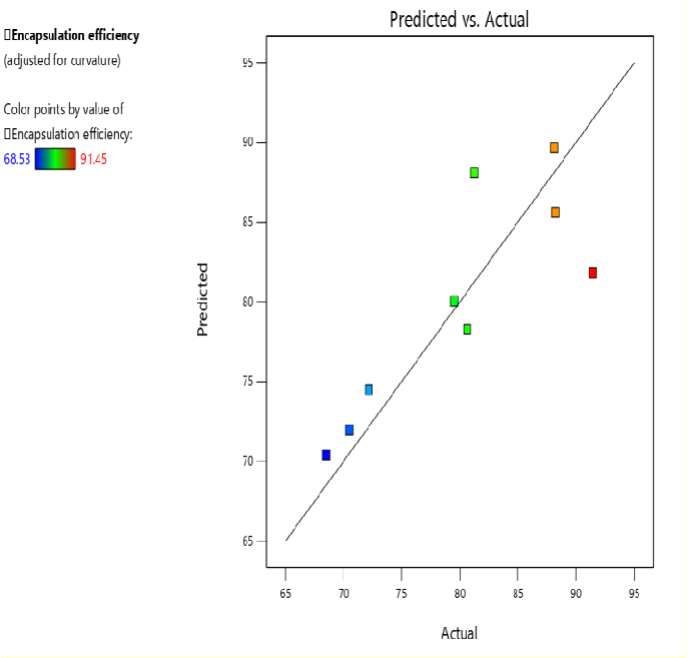

Figure13.Predicted versus actual plot showing the correlation between experimentally observed values and model-generated values for the nanogel response. The close clustering of data points along the diagonal line confirms the accuracy, reliability, and goodness-of-fit of the developed statistical model

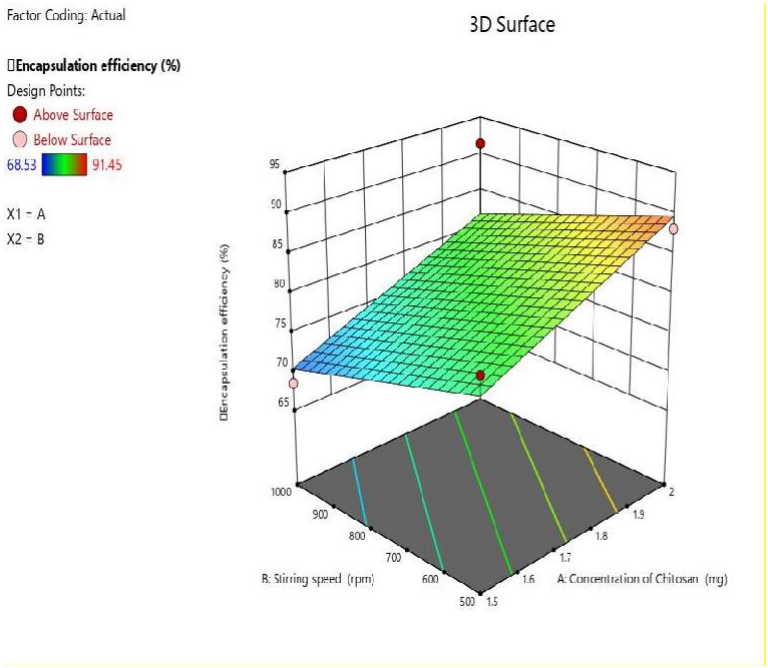

Figure14.Three-dimensional response surface plot depicting the combined influence of Chitosan concentration (A) and Stirring speed (B) on the nanogel response. The curvature of the surface illustrates how factor interactions affect the response and highlights the optimal operational region identified through QbD-based optimization

3.4 Surface morphology by Transmission electron microscopy(TEM)

The TEM analysis of formulation L8 revealed well-defined, spherical nanoparticles with a uniform morphology and an approximate size of 84 nm, confirming successful nanoscale fabrication. The smooth surface and discrete particle distribution indicate good structural integrity and minimal aggregation. These findings support the efficiency of the formulation method in producing stable nanoparticles within the desired size range, which is essential for enhancing drug encapsulation, release behavior, and overall therapeutic performance. Thus, the TEM results validate the suitability of formulation L8 for further characterization and potential pharmaceutical application.

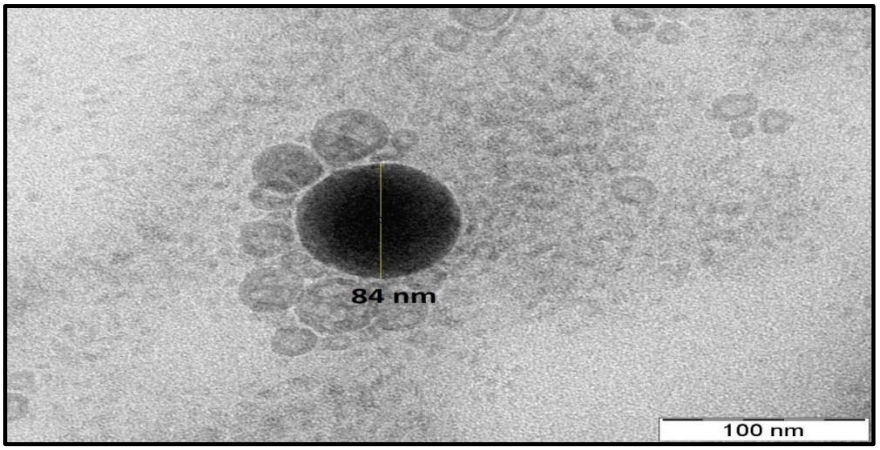

Figure. 15 TEM image of optimized batch L8

3.4.1 PXRD study

The XRD pattern of formulation L8 displayed sharp peaks at 2θ values of 11.2°, 16.2°, 21.9°, and 24.5°, confirming its crystalline nature. The dominant peak at 21.9° suggests strong crystalline reflections, attributable to the drug and/or excipients, indicating that the formulation retains a predominantly crystalline profile.

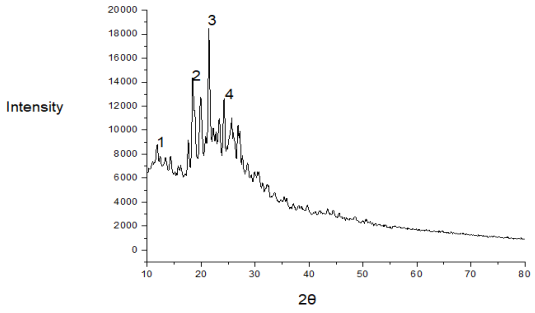

Figure. 16 Diffractogram of optimized batch L8

3.5. Invitro drug release

Table 9.Invitrodrugrelease

Time (min)	L1	L2	L3	L4	L5	L6	L7	L8	L9
0	0	0	0	0	0	0	0	0	0
15	8.5±0.02	10.3±0.14	18.4±0.11	20.1±0.23	9.6±0.14	14.2±0.11	12.4±0.11	21.6±0.11	15.0±0.14
30	14.9±0.12	20.7±0.17	30.2±0.21	35.3±0.22	17.3±0.21	25.4±0.20	21.6±0.15	38.5±0.14	27.9±0.24
60	25.7±0.13	34.5±0.22	48.1±0.14	56.8±0.12	30.5±0.11	42.8±0.28	37.9±0.21	60.9±0.11	45.3±0.14
90	32.6±0.11	44.8±0.24	59.7±0.11	72.4±0.11	41.1±0.22	55.6±0.12	50.3±0.19	74.1±0.20	59.6±0.15
120	39.2±0.8	52.3±0.25	69.8±0.20	84.7±0.7	50.2±0.23	66.3±0.14	61.5±0.17	85.4±0.24	70.8±0.24

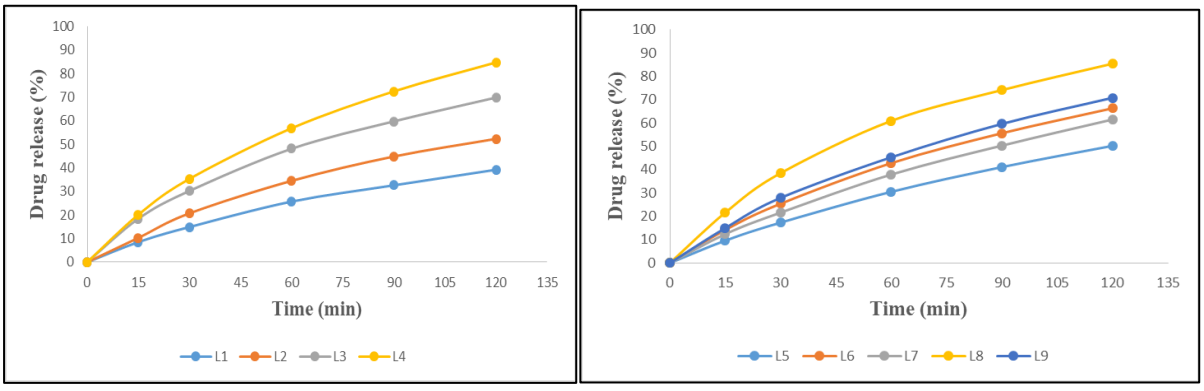

(a) (b)

Fig 17. % (a) Drug release from L1-L4, (b) Drug release from L5-L9

3.5.1 Stability studies

Table10. Stability studies

Time (Months)	Physical Appearance	Viscosity (cP)	Drug Release (%)
0	Clear, colourless gel	5980 ± 45	85.42 ± 0.15
1	No change	5970 ± 42	85.05 ± 0.17
2	No change	5975 ± 40	85.10 ± 0.19
3	No change	5960 ± 44	85.11 0.14
			85.12

3.6 In vivo animal study (Wound Healing)

Table 11. Original Wound Area

Groups (n= 06)	Treatment periods (days)					
	Total wound area	1st day	3rd day	7th day	14thday	21th day
Group I (F1=CONTROL)	334.58 ± 12.25	341.58 ± 12.39	330.54 ± 54.36	326.04 ± 89.23	321.54 ± 52.38	256.04 ± 83.56
Group II (F2 =standard)	396.19 ± 43.56	388.27 ± 78.25	299.10 ± 54.21	224.73 ± 78.63	182.10 ± 45.62	79.56 ± 12.35
Group III (F3 =optimized formulation(L8)	365.07 ± 56.25	357.48 ± 38.69	278.63 ± 45.21	208.05 ± 45.36	196.23 ± 41.25	122.39 ± 21.35

Table 14 % Wound Contraction

Groups (n= 06)	Treatment periods (days)				
	1st day	3rd day	7th day	14thday	21th day
Group I (F1=CONTROL)	1.09 ± 0.36	1.20 ± 0.23	1.20 ± 0.12	2.54 ± 0.23	23.49 ± 0.87
Group II (F2 = Standard)	1.68 ± 0.19	2.00 ± 0.12	24.49 ± 0.98	43.30 ± 0.29	79.91 ± 0.98
Group III (F3 =Optimized Formulation(L8)	1.67 ± 0.48	2.08 ± 0.28	23.70 ± 0.85	43.01 ± 0.28	66.48 ± 0.58

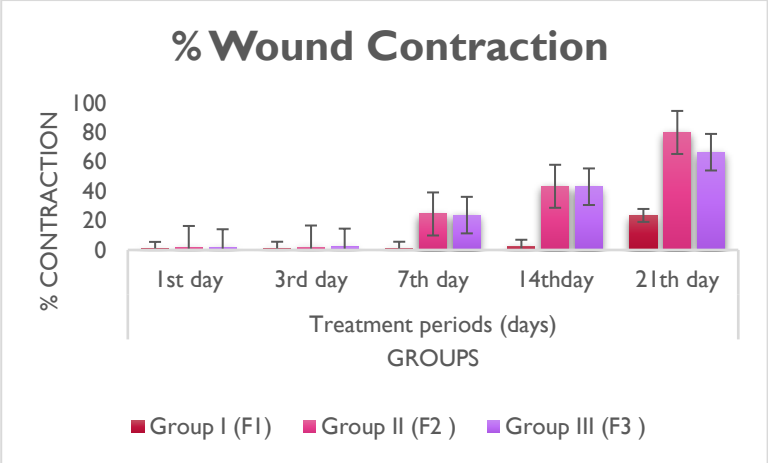

Fig 18. Wound Contraction

The optimized formulation (L8) showed significant wound healing activity in excision model. In the excision model, it achieved 66.48% wound contraction by Day 21 versus 23.49% in control and close to the standard (79.91%).indicating improved collagen deposition and epithelialization. Overall, the formulation enhanced wound closure and tissue regeneration, confirming its therapeutic potential.

CONCLUSION

Silver nanoparticles (AgNPs) with antibacterial and durable characteristics were produced extracellularly by Bacillus licheniformis, a non-pathogenic microbe. This study added biosynthesized AgNPs to a nanogel, a three-dimensional hydrophilic polymeric network that improves drug loading, release, and retention at the target location. Nanogel was improved for therapeutic efficacy, tissue infiltration, and wound healing. The modified formulation was tested for physicochemical properties, in-vitro research, and in-vivo wound healing in albino Wistar rats using excision wound model. Wound contraction, epithelialization, were higher than control and standard formulations, indicating better wound healing.

REFERENCES

1. Tufail S, Liaqat I, Ali S, Ulfat M, Shafi A, Sadiqa A, Iqbal R, Ahsan F. Bacillus licheniformis (MN900686) Mediated Synthesis, Characterization and Antimicrobial Potential of Silver Nanoparticles. J Oleo Sci. 2022;71(5):701-708.
2. Paramasivam G, Dhanasekaran S, Kalpana D, Mohan R. Nanomaterials – synthesis, characterization, recent advances and applications: A review. J King Saud Univ Sci. 2021;33(2):101322.
3. Zafaryab, M., & Vig, K. (2025). Biomedical Application of Nanogels: From Cancer to Wound Healing. Molecules, 30(10), 2144.
4. Joudeh N, Linke D. Nanoparticle classification, physicochemical properties, characterization, and applications: a comprehensive review for biologists. J Nanobiotechnology. 2022;20(1):262.
5. Hao J, Liu X, Du Y. Fabrication of gelatine/fucoidan nanogel-coated silver nanoparticles for the treatment of wound healing therapy and nursing care. Regen Ther. 2025 Mar 29;29:282-291.
6. Mohammed-Sadhakathullah A, Alzahrani S, Alharbi SA, Abdulhakeem BH, Ameen F. Recent advancements and biological prospects of organic nanoparticles in drug delivery systems: a comprehensive review. Biomed Pharmacother. 2023;162:114637.
7. Gupta M, Shrivastava B, Ghuge A, Dand N. *Formulation and Evaluation of Nanosponge-based Drug Delivery System of Aceclofenac for Topical application.* Research Journal of Pharmacy and Technology. 2023;16(12):5713-5721.
8. Mekkawy A. I., El-Mokhtar M. A., Nafady N. A., Yousef N., Hamad M., El-Shanawany S. M., Ibrahim E. H., & Elsabahy M. (2017). *In vitro and in vivo evaluation of biologically synthesized silver nanoparticles for topical applications: Effect of surface coating and loading into hydrogels.International Journal of Nanomedicine*, 12, 759–777..
9. **Chen M, Pan X, Wu H, et al.** Preparation and anti-bacterial properties of a temperature-sensitive gel containing silver nanoparticles. *Pharmazie.* 2011; 66(4): 272–277.Laroui H, Dalmasso G, Yan Y, Nguyen HT, Sitaraman SV, Merlin D. Drug-loaded nanoparticles targeted to the colon with polysaccharide hydrogel reduce colitis in a mouse model. Gastroenterology. 2013;145(3): 500–511.e3.
10. **Annisa R., Suryadinata A., Nashichuddin A., Fauziyah B., Mutiah R., Hendrawan N. Z.** Development of an antimicrobial gel formulation for topical delivery using silver nanoparticle. *Indian Journal of Novel Drug Delivery.* 2019; **11**(1): 13–19.
11. Mehta A, Jain A, Jain SK. Nanobots: the future of medicine. Int J Pharm Sci Res. 2012;3(10):3574–3580.
12. **Jain J, Arora S, Rajwade JM, Omray P, Khandelwal S, Paknikar KM.** Silver nanoparticles in therapeutics: Development of an antimicrobial gel formulation for topical use. *Molecular Pharmaceutics.* 2009; 6(5): 1388–1401.
13. Sabale V, Vora S. Formulation and evaluation of microemulsion-based hydrogel for topical delivery. International journal of pharmaceutical investigation. 2012 Jul;2(3):140.
14. Rane BR, Patil RS and Jain AS: Formulation development and evaluation of nanogel loaded with montelukast sodium niosomes. Int J Pharm Sci & Res 2021; 12(8): 4208-21. doi: 10.13040/IJPSR.0975-8232.12(8).4208-21.
15. Kesharwani P, Jain A, Srivastava AK, Keshari MK. Systematic development and characterization of curcumin-loaded nanogel for topical application. Drug development and industrial pharmacy. 2020 Sep 1;46(9):1443-57.
16. Patel VR, Patel PG, Patel KR, Patel NM. Formulation and development of nanogel containing green tea extract: as topical dosage form. Int J Pharm Sci Res. 2011;2(8):2162-2168.
17. Phatak AA, Chaudhari PD. Development and evaluation of nanogel as a carrier for transdermal delivery of aceclofenac. Asian Journal of Pharmacy and Technology. 2012;2(4):125-32.
18. Pekmez M, Milat NS. Evaluation of In Vitro Wound Healing Activity of Thymoquinone. Eur J Biol 2020; 79(2): 151-156. DOI: 10.26650/EurJBiol.2020.0044.
19. **Kaler A, Mittal AK, Katariya M, Harde H, Agrawal AK, Jain S, Banerjee UC.** An investigation of in vivo wound healing activity of biologically synthesized silver nanoparticles. *Journal of Nanoparticle Research*. 2014;16:2605.
20. Aydın, P., Karaköy, Z., & Halıcı, H. (2024). Evaluation of Wound Healing Potential of Galangin on L929 Mouse Fibroblast Cell Lines Using In Vitro Scratch Assay. Current Research in Health Sciences, 1(3): 99-104.
21. **Özdemir K. G., Yılmaz H., & Yılmaz S.** In Vitro Evaluation of Cytotoxicity of Soft Lining Materials on L929 Cells by MTT Assay. *Journal of Biomedical Materials Research Part B: Applied Biomaterials.* 2009; 90(1): 82–86. doi:10.1002/jbm.b.31256.
22. **Rigo, C., Ferroni, L., Tocco, I., Roman, M., Munivrana, I., Gardin, C., et al.** (2013). Active silver nanoparticles for wound healing. *International Journal of Molecular Sciences*, **14**(3), 4817–4840